International Journal of Refractory Metals and Hard Materials 130 (2025) 107163

Contents lists available at ScienceDirect

International Journal of Refractory Metals and Hard Materials

journal homepage: www.elsevier.com/locate/IJRMHM

Investigation of wear and corrosion resistance of WC-coated Pearlitic railway steel in dry and wet conditions

Abdulkadir Orak [a,*], Seyma Korkmaz [b], M. Huseyin Cetin [c]

[a] Yalova University, Department of Mechanical Engineering, 78050, Yalova, Turkey
[b] Kırsehir Ahi Evran University, Department of Electronics and Automation, 40100 Kırsehir, Turkey
[c] Konya Technical University, Department of Mechanical Engineering, 42250 Konya, Turkey

ARTICLE INFO

Keywords:
WC coating
Railway steel
Wear
Corrosion

ABSTRACT

In this study, the effect of WC coating on the tribological performance of R260 rail steel was investigated by roller-on-plate wear tests and potentiodynamic polarisation corrosion tests carried out in dry and pure water environments. The High-Velocity Oxygen-Fuel (HVOF) method was used for the coating process. The tests were conducted with a weight of 40 N and a sliding speed of 0.03 m/s. An Ag/AgCl reference electrode was also used for corrosion tests in a 3.5 % NaCl solution. To produce cyclic polarisation curves, the experiments were carried out at a scan rate of 1 mV/s within a potential range of ±0.25 V. The effect of WC coating on the wear performance of rail steels was analysed quantitatively with the friction coefficient and volume loss parameters and visually with SEM and 2D-3D topography images. The effect of the coating on the corrosion performance was evaluated numerically with the corrosion potential, corrosion current intensity, and corrosion rate values, as well as elementally and visually with SEM and EDX images. Wear test results showed that the wear volume in WC-coated rail steels decreased by 43.07 % and 46.94 % compared to uncoated rail steels in dry and wet conditions. Corrosion test results showed that the corrosion rate of WC-coated rail steels was lower compared to uncoated rail steels, and the corrosive effect spread to a smaller area.

1. Introduction

Sustainability in transportation can be achieved by optimising economic and safety parameters [1,2]. To achieve the combination of maximum safety and minimum cost, the service life and operating performance of system components must be increased [3,4]. In recent years, technological developments in railway transportation have increased the demand for increased load/passenger capacities (axle load) and high speeds [3,5–7]. Due to increasing axle load and speed, the stresses at the wheel-rail interface increase and cause deformation of system components. Due to deformation, operating performance, safety and passenger comfort are negatively affected. Considering the problems mentioned, deformation formation must be minimised in order to increase system performance and safety. The most common deformations occurring on rails in railway transportation are caused by wear, fatigue and corrosion due to wheel-rail contact [3,8–12].

Considering the mechanical properties of existing rail steels, the weldability and fatigue strength of pearlitic rail steels have increased their preferability compared to others [13,14]. In addition, pearlitic rail steels are widely used due to their ability to provide the optimum combination of strength and toughness [6,13]. Chromium-manganese-based rail steels are special rail steels developed for high wear and corrosion resistance [15,16]. For this reason, chromium-manganese-based pearlitic microstructured R260 rail steel was determined as the reference rail in this study [17–19]. R260 rail steels have high wear resistance due to the hard cementite in their microstructure [20]. However, the spheroidization of cementite lamellar due to local heat formation in the internal structure of pearlitic rail steels reduces the material's wear resistance [21]. Especially in repeated accelerations, sliding motion during skidding, braking and skidding in curve and switch regions increases friction [3,21]. Thermal loads resulting from increased heat caused by friction cause plastic deformation. Corrugation and damage defects occur on the rail surface due to plastic deformations [22]. These defects cause noise in the short term and reduce passenger comfort while shortening the service life of the rail in the long term [23]. It is known that the rail life, which is 20–25 years on straight sections of the railway line, decreases to 2–3 years on curves due to deformations caused by wear [24,25]. One of the important factors affecting the

* Corresponding author.
E-mail address: abdulkadir.orak@yalova.edu.tr (A. Orak).

https://doi.org/10.1016/j.ijrmhm.2025.107163
Received 19 October 2024; Received in revised form 26 February 2025; Accepted 21 March 2025
Available online 22 March 2025

service life of rails is corrosion-induced deformations [10]. Macroscopic pits form on the rails due to heavy axle loads in contact with rain and snow water [26]. In addition, the presence of NaCl in railways close to the sea and the acidic environment (H_2SO_4) occurring in tunnels due to atmospheric changes increase corrosion and negatively affect the mechanical properties of pearlitic rail steels [8]. For this reason, wear and corrosion defects occurring on the rail surface should be minimised.

According to literature studies, it has been determined that different surface treatments increase the wear and corrosion resistance of rail steel [14,27,31–33]. It has been proven that hardness and tensile strength are increased without affecting the material's toughness by rapidly cooling the rail mushroom and that wear can be reduced with appropriate surface treatments in small radius curves [3,7]. However, it is important to obtain optimum hardness in rail steel in these surface treatments. Otherwise, the increase in microhardness on the rail mushroom surface causes martensitic transformation, increasing the material's brittleness and reducing the wear resistance [17]. In addition, corrugation may occur in the case of heat-treated rails, which may cause wavy wear [34,35]. When studies examining the corrosion behaviour of rail steel are evaluated, it has been observed that microstructure change affects corrosion resistance, and the pearlitic structure increases corrosion resistance [33,36]. However, it is observed that pitting and microcrack deformations due to corrosion occur in rail steel under rainwater and heavy load conditions [30,37]. If these deformations are not maintained, repaired or replaced, the safety of the line decreases, and this causes serious accidents. Due to the disadvantages of heat treatment methods, coating is preferred as an alternative [38,39].

In current literature studies, it has been determined that the wear and corrosion resistance of rail steels coated with the laser method increases [40–42]. In existing studies, mostly cobalt-based Stellite and steel materials were used as coating material, and the experiments were carried out only in dry conditions [34,43,44]. Rail steels are exposed to rain and snow water as well as dry conditions. However, few studies investigate the wear and corrosion behaviours of coated rail steels in wet conditions.

The original value of this study is the increase of the wear and corrosion resistance of rail steels exposed to atmospheric effects with the WC coating process. This study is especially important for minimising catastrophic wear occurring on rails used in switches and curves. Within the scope of the study, uncoated and WC-coated pearlitic structured R260 rail steels were subjected to roll-on-plate wear tests in dry and pure water environments, 40 N load and 50 rpm speed parameters for the analysis of wear behaviour. It is important to carry out wear tests in a rolling friction environment in order to simulate operating conditions. The results were evaluated by comparing the friction coefficient and wear volume values. A test was performed to analyse the corrosion behaviour occurring in a pure water environment, and a Tafel graph was obtained. 3D topography images and surface roughness values obtained from worn surfaces were analysed for surface morphology analysis. Additionally, SEM, EDX and XRD images obtained from worn and corroded surfaces were examined.

2. Material and experimental method

2.1. Material

R260-type rail steel was used in the experiments, and its chemical composition is shown in Table 1. R260 rail steel was preferred in the study because it is the most widely used rail material today and exhibits superior tribological performance compared to other rail steels [17,43]. R260 rail steel is a chrome-manganese-based steel with a pearlitic structure and high wear and corrosion resistance [6]. The spheroidization of the cementite phase in the pearlitic structure under the effect of heat reduces the wear resistance of the rail [21]. For this reason, within the scope of the study, the wear resistance of R260 rail steel was tried to be increased with WC-Co coating. It was anticipated that the obtained results would also be a reference for other rail steels. Wear tests were carried out in the rail-head area of the samples (Fig. 1). Before the coating process and wear tests, the sample surfaces were cleaned using 200–400–800-1000 numbered sandpapers to remove the oxide layer on the surface.

Wear samples were prepared in dimensions of 40 mm × 10 mm × 10 mm. To increase the tribological performance of R260 rail steel, the head area of the rail was coated with tungsten carbide material. Tungsten carbide is widely used, especially in industrial applications subject to sliding wear, because it increases the hardness of the materials as well as the wear and corrosion resistance [45,46]. With technological developments, the increase in passenger/load capacity and travel speed in railway transportation increases the possibility of deformation of the rail material [3,5–7]. WC material was preferred due to its high mechanical and tribological properties. Cobalt (Co) was used as the binder material to ensure sufficient adhesion between WC and rail steel [47,48]. Cobalt can interact well with the carbides of Group 6 elements and provide high wettability and solubility performance on the surface [49]. Thanks to the ductile Co reinforced to the WC material, a coating layer with high fracture toughness, hardness and corrosion resistance is formed on the surface [47,50–53]. The reinforced Co ratio was determined as 12 % considering the literature [48,54] studies and industrial applications [47,48,55–57]. WC-Co coating process with a thickness of 160±40 μm was applied to the surface of the rail steel with a hardness value of 261 HV by the high-speed oxide-fuel (HVOF) coating method. The fact that the HVOF method is performed under high-impact speed and low-temperature conditions reduces decarburisation compared to other thermal spraying methods [45,53,55,56,58,59]. Low-cost applications and the absence of adverse ecological effects are important factors that increase its use in industrial applications [60]. The HVOF method was preferred in the present study, considering tribological-mechanical performance and economic-environmental factors. The HVOF process

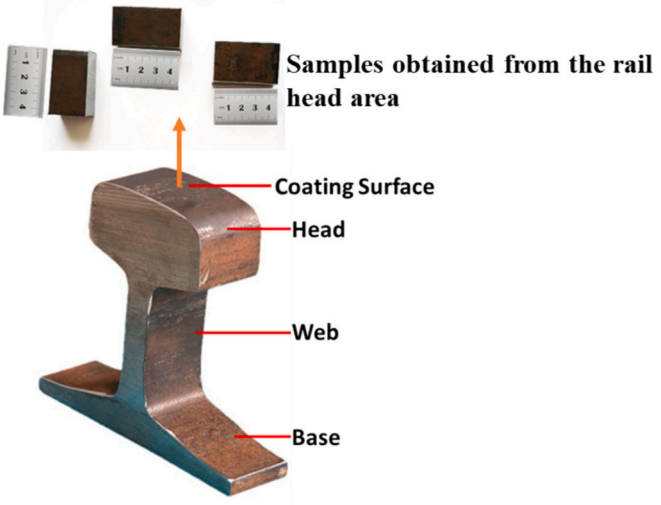

Fig. 1. R260 type rail steel (Studio photograph).

Table 1
Chemical composition of R260 rail steel.

Element	C	Mn	Si	Cr	Mo	S	P	Fe
Weight %	0.74	1.25	0.35	0.12	0.035	0.018	0.015	Balance

was carried out using a Metco Diamond Jet 2700 type gun with the parameters of 10 bar oxygen pressure, 90 °C substrate temperature, 350 mm spraying distance and 30 g/min powder feeding rate. The microhardness values of the samples were measured with the Bruker UMT Universal hardness tester; the values obtained are given in Table 2. The hardness values were calculated by taking the average after six measurements.

2.2. Experimental method

Roller-on-plate type tribometer was used in the experiments. The experimental parameters and photographs of the wear test device are shown in Table 3 and Fig. 2. In the roller-on-plate system, the abrasive ball was left free to make a rolling motion, and the rail-wheel friction was attempted to be simulated [28]. In the wear tests of uncoated and WC-coated rails, 6 mm diameter spherical 100Cr6 (AISI 52100) with a hardness of ~700 HV was used as the abrasive material. Wear tests were carried out for 16,667 cycles (1000 m) at 40 N load and 0.03 m/s speed parameters. The load and speed parameters were determined using the literature data and preliminary experiments [32,61–63]. The experiments were conducted in a pure water environment to simulate dry and atmospheric conditions. The ambient temperature where the experiment was carried out and the pure water temperature were ~ 23 °C. In the measurements made during the experiments, it was determined that the ambient and water temperatures showed negligible changes. The volume of pure water in which the experiments were carried out was 300 ml.

SEM imaging, elemental analysis (EDX) and microhardness measurement methods were used to characterise the coated samples. Linear method and mapping method were used in the EDX analysis. A dynamometer with ±0.1 N sensitivity was used to measure the coefficient of friction. The friction forces (axial force) measured with the dynamometer were divided by the load acting on the material to obtain the kinetic friction coefficient values. The friction coefficient was obtained every 0.14 m along the 1000 m wear path and graphed. Approximately 7000 friction coefficient values were calculated, and the arithmetic average of these values was considered. SEM (CARL ZEISS GEMINI FESEM), EDX and 3D topography (Phase View Optical Profilometer) imaging methods were used for surface morphology analysis. For the quantitative analysis of the deformations occurring on the surface, the width (a) and depth (b) values of the wear scar were determined from the wear profile images obtained with the 2D profilometer and the stroke distance (c) was measured with the help of a calliper (Fig. 3). Using the obtained width, depth and stroke distance values, wear volume values were calculated with the help of the equation given in Eq.1.

$$V = \frac{2}{3}.a.b.c \tag{1}$$

Uncoated and WC-coated samples were subjected to a potentiodynamic polarisation (Tafel method) test to analyse the effect of WC coating on corrosion resistance. Corrosion potential and corrosion current density can be determined easily and quickly with the Tafel method, and reliable results can be obtained even at low corrosion rates [64]. For this reason, the Tafel method was preferred in the present study. Tests were carried out using a 3.5 % NaCl solution and at room temperature using the Parstat 4000 model electrochemical impedance spectroscopy. Ag/AgCl, platinum, and three-electrode cells were used as reference electrodes, counter electrodes, and working electrodes, respectively. Polarisation curves were obtained with cyclic measurements applied at 1 mV/s scanning speed and ± 0.25 V potential range. Corrosion potential and corrosion current density values were determined with the help of curves in "semi-logarithmic current density-potential" graphs created as a result of measurements (Tafel extrapolation method).

Table 2
Hardness values of samples.

Type of Sample	Hardness (Vickers)
Uncoated Sample	263 ± 2 HV
WC-Co Coated Sample	1270 ± 11 HV

Table 3
Corrosion test results.

Specimen	I_{corr} (A/cm^2)	CR (mm / year)	E_{corr} (V)
Uncoated Railway Steel	1.48×10^{-6}	0.017	−0.441
WC Coated Railway Steel	4.21×10^{-7}	0.005	−0.613

3. Results and discussion

The results were investigated in two stages: metallurgical and tribological characterisation of WC-Co coated rails. In metallurgical characterisation, hardness measurement and SEM, XRD, and EDX (line and mapping) images were analysed. To investigate the effect of WC-Co coating on corrosion behaviour, Tafel polarisation curves obtained by the potentiodynamic method were examined, and the corrosion effect on the surface was analysed by SEM images. In tribological characterisation, friction coefficient values obtained during wear tests and volume loss values after wear were examined, and surface morphology was investigated by SEM and 3D topography images.

3.1. Characterisation of WC coating layer

Carbide-based coatings are of interest in improving the surface properties of engineering materials. Interstitial solid solutions formed due to the ~0.071 nm atomic radius of carbon can increase the tribological performance of materials exposed to wear with their high hardness properties [65]. Homogeneous coating thicknesses can also be obtained depending on the stability of the coating process. The cross-sectional view of WC-12 %Co material coated with HVOF on R260 rail steel is given in Fig. 4. Fig. 4.a shows the pearlitic microstructure, and Fig. 5.b shows an average 165 μm WC coated section on the pearlitic structure. It is seen that the coating forms a wavy surface due to its high thickness. Similar forms have been observed in the literature on WC-coated surfaces [66]. It can be said that a wavy form is formed on the surface depending on the spraying speed of the HVOF method. The high spraying speed in the HVOF method creates a shot-peening effect and makes the surface wavy. However, the fine-grained structure formation seen in shot peening processes was not observed in the internal structure. No microstructure change occurred due to the short duration of the HVOF process and the formation of a WC layer on the surface during the process. According to the SEM image, it was determined that there were minimal cracks, voids and tear defects in the coating layer. Considering the thickness of the coating layer, it can be claimed that the defects formed were negligible. Fig. 4.b shows homogeneously distributed WC particles in a 12 % cobalt matrix. It is understood from the elemental mapping image that despite the high tendency of WC particles to clump, a homogeneous distribution was achieved thanks to the cobalt binder.

The EDX analyses performed for the analysis of coating quality are given in Fig. 5. In Fig. 5.a, an intense carbon peak originating from the oxide layer is observed on the surface of the uncoated sample. It is observed that the carbon distribution on the rail material surface becomes homogeneous after the coating process. It can be said that the oxide layer is dispersed due to the pressure and temperature in the coating process and the decarburization effect [55]. The dominant elements (C, W, Co) seen in Fig. 5.b are distributed homogeneously throughout the coating layer. Depending on this situation, it can be claimed that the coating is of sufficient quality in terms of spectral. In addition to the elemental homogeneity of the coating, the bond it forms with the base material is also important. It is seen in the XRD graph in Fig. 6 that the Fe_3W_3C alloy is formed depending on the solid-state solution formed with the base material. It can be claimed that a stable

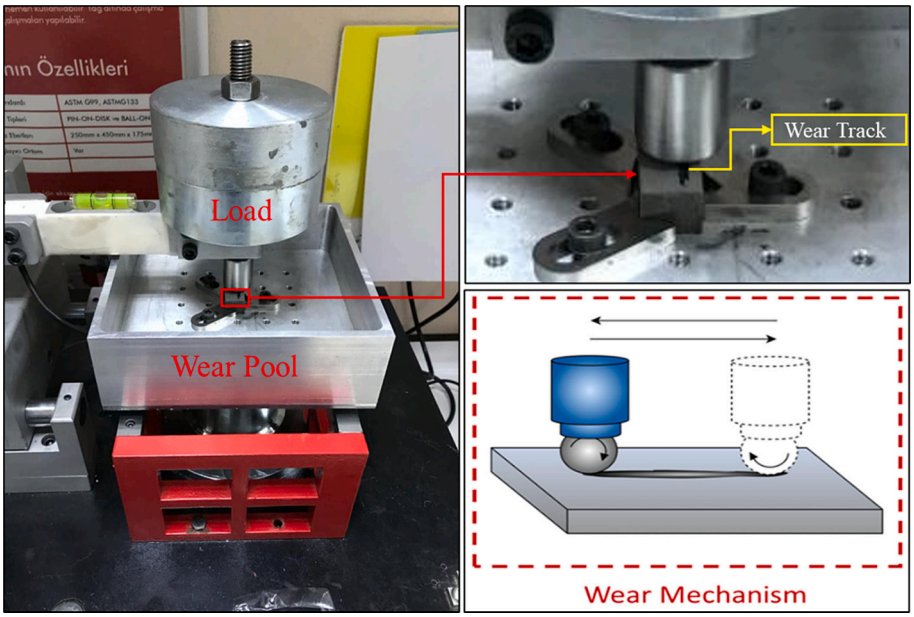

Fig. 2. Photograph of the wear test unit.

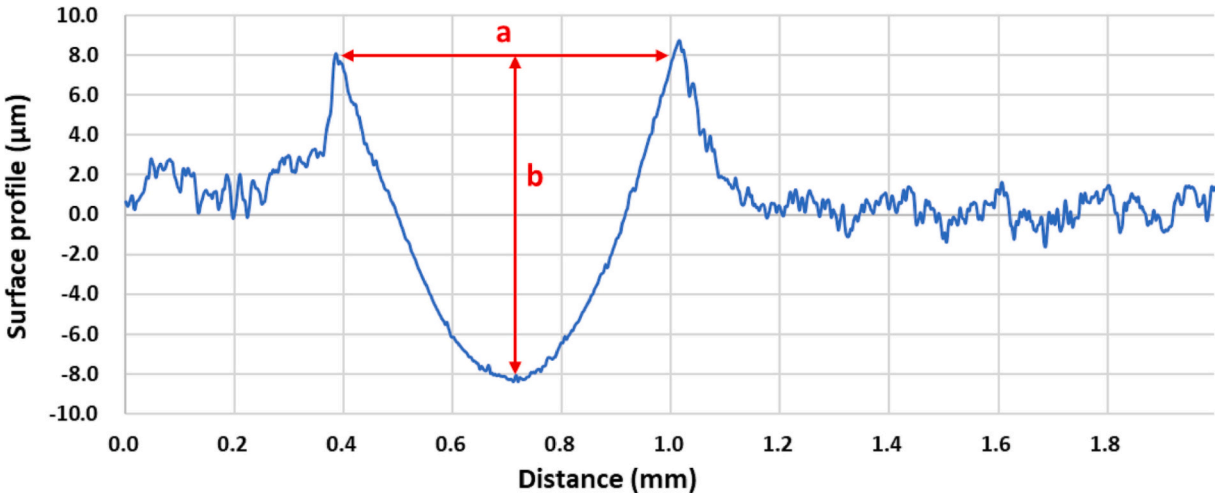

Fig. 3. An example of a wear profile was obtained with the 2D profilometer.

bond formation occurs thanks to the cubic crystal lattice structure of the alloy. The formation of the WC and W_2C peaks seen in Fig. 6 is an expected situation for tungsten-coated alloys.

In the coating images given in Fig. 4 and Fig. 5, it is seen that there is no colour change or tone difference for WC and W_2C. However, according to the microhardness graph given in Fig. 7, it is observed that the W_2C layer (hardness between 1250 HV and 819 HV) is formed on the surface of the material first, and then the WC layer, which reaches an average hardness value of 750 HV, is formed. While the average hardness value for W_2C is 1052 HV, the average hardness value for WC is 752 HV. The deviation value in the measurements is around 2 %. While no change is observed in the hardness value along the WC layer, the hardness value in the W_2C layer decreased due to decarburisation. It can be said that there is variability in the hardness layer depending on the oxidation rate and HVOF parameters. Another remarkable situation in the hardness graph is that the transition zone occurs at a distance of ~50 µm. The hardness value decreased from 750 HV to 340 HV in this region. This trend can be evaluated as problematic in terms of coating strength. Thanks to the fast drop, stress concentrations may occur due to hardness changes during the material's force flow, and the coating layer's service life will be adversely affected. However, it can be claimed that thanks to the diffusion-enhancing effect of HVOF process parameters, the problems that may occur in terms of the transition zone will be minimised.

3.2. Tribological performance of the WC layer under dry and pure water conditions

For tribological performance analysis, firstly the friction coefficient data were examined (Fig. 8). The variation of friction coefficients showed a consistent fluctuation for all conditions. The arithmetic average of the values in the variation graph was taken into account. According to Fig. 8, the friction coefficient of the uncoated rail sample in a pure water environment decreased by 23 % compared to the dry environment. This situation can be explained by the film layer formed by pure water in the roughness region of the wear interface. With the effect of the film layer, the compressive and shear stresses formed during friction decreased, and the friction coefficient decreased. The values obtained in the water environment are important for analysing the effect of the coating. It was determined that the friction coefficient values of

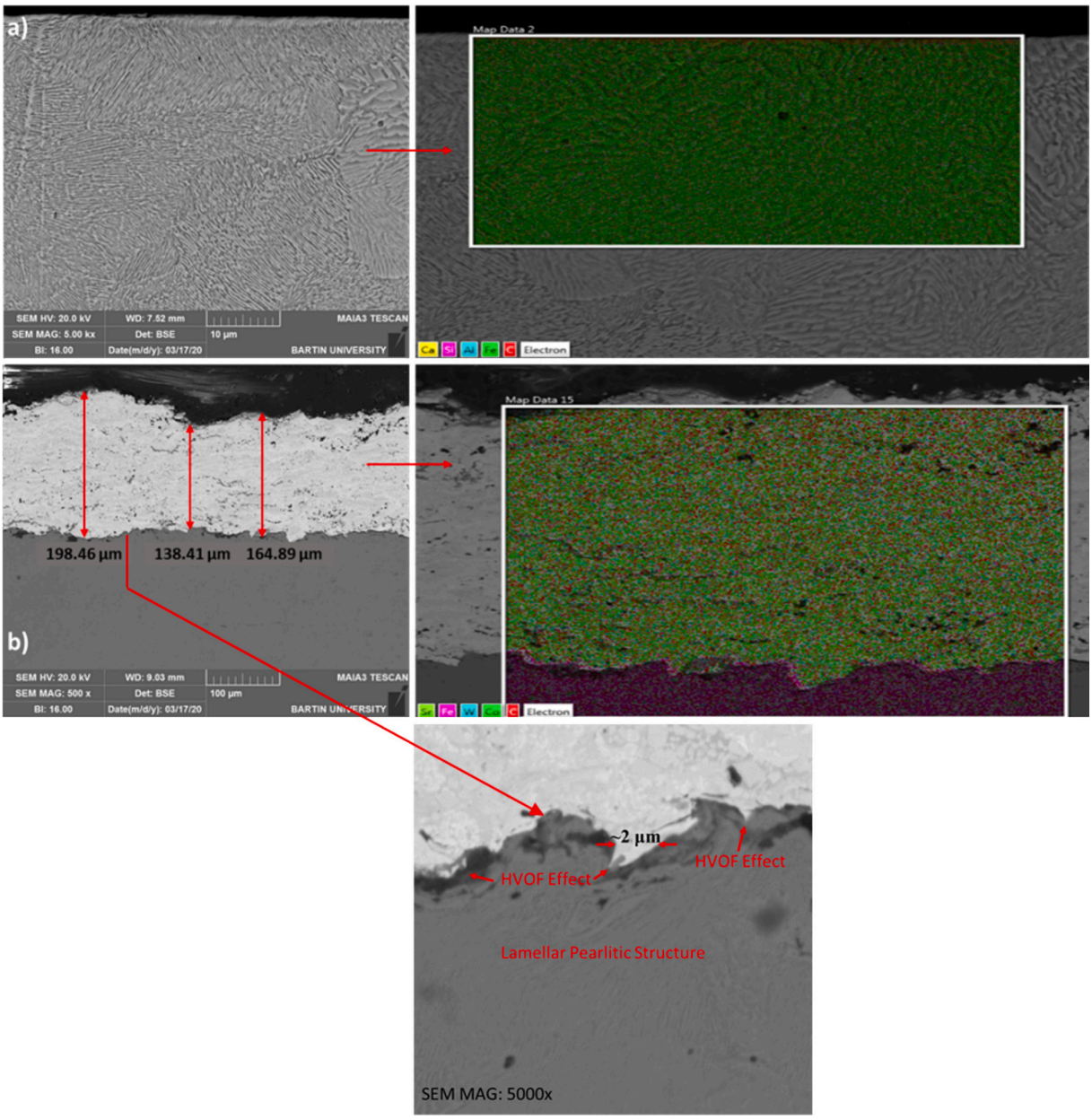

Fig. 4. (a) Pearlitic rail steel microstructure image (b) Cross-sectional image of WC coating on pearlitic rail steel.

the WC-coated sample in a dry environment and the uncoated sample in a pure water environment were the same. This situation shows that the ~750 HV hardness increase created a liquid film layer effect. The fact that the hardness increased from 260 HV to an average value of 1000 HV with the coating provided a 23 % decrease in the friction coefficient. The decrease in the friction coefficient shows that the WC coating is effective and applicable for reducing the amount of friction on the rails. According to Fig. 8, the friction coefficient value of the coated sample in pure water conditions decreased by 34.78 % compared to the uncoated sample, and the friction coefficient value of the coated sample in dry environment conditions decreased by 30.43 % compared to the uncoated sample. The coating process significantly reduced the friction coefficient.

The decrease in the coefficient of friction as a result of WC coating is not significant in terms of the adhesion between the rail and the wheel. The adhesion value, which expresses the ability of the wheel to hold onto the rail, is expected to decrease with the decrease in the coefficient of friction [67]. For this reason, WC coating cannot be applied along the rail line due to technical and economic requirements. However, WC coating can be used where sliding friction occurs on the rail instead of rolling friction. Especially in switch transitions and curves, catastrophic deformations can occur due to the intense sliding friction [68]. Reducing the coefficient of friction with WC coating in these areas is important in terms of minimising deformations.

WC coating has a hexagonal close-packed structure (hcp), while rail steel has a body-centred cubic (bcc) crystal lattice structure [69,70]. Most engineering materials that can form qualified alloys have HCP and BCC crystal structures. Especially under pressure and temperature, i.e. in environments where high energy input is made to the material, the bond formation between hcp and bcc structures accelerates [71]. It can be claimed that the bond strength between the coating and the rail steel will increase due to the increased pressure and temperature between the rail and the wheel as a result of the continuous contact of the train with the railway line. In WC-coated areas where sliding friction occurs, increasing temperature and pressure can increase the bond strength of the WC coating and provide an additional contribution to the wear

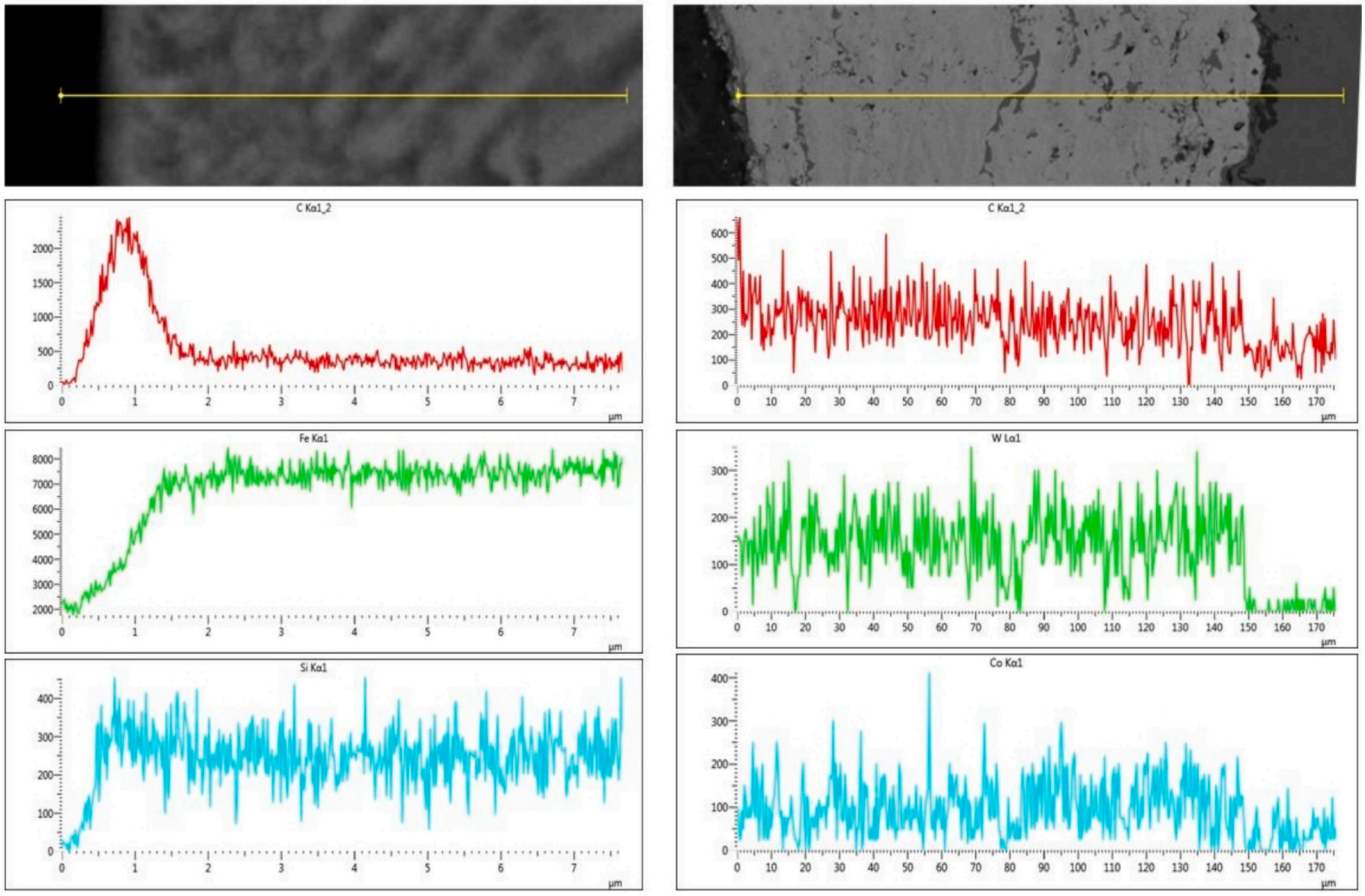

Fig. 5. EDX images (a) uncoated sample (b) WC coated sample.

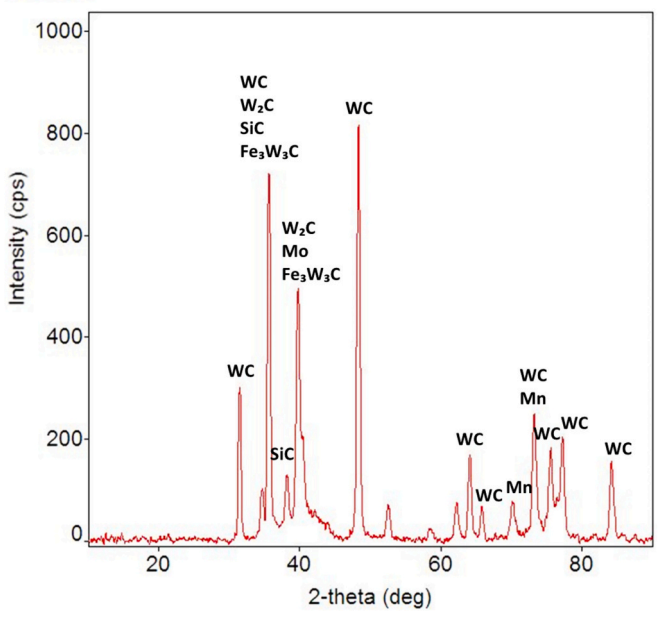

Fig. 6. XRD graphic image of WC-coated samples.

resistance. In this way, the secondary wear periods of engineering materials will increase. In areas where rail deformation is intense, reducing the friction coefficient with WC coating and extending the secondary wear period of the coating due to the energy input during the train passage is meaningful in terms of increasing the service life of the rail. However, the coating thickness will decrease in the long term due to the deformations formed on the coating surface.

The roughness images obtained with the 2D profilometer for the wear volume analysis are given in Fig. 9. According to Fig. 9, the wear volume value of the coated sample in pure water conditions decreased by 46.94 % compared to the uncoated sample. In dry environment conditions, the wear volume value of the coated sample decreased by 43.07 % compared to the uncoated sample. The coating process significantly reduced the wear volume. While a distinct wear pit formation was observed in the uncoated samples, it was observed that no distinct wear marks were formed in the WC coated samples. However, it was determined that the wear mark depth in the coated samples progressed up to 15 µm in dry and pure water environments (Fig. 9.c and Fig. 9.d). Considering the average coating thickness of ~150 µm, it is seen that a 10 % wear depth was formed. It can be claimed that due to the excessive hardness on the surface of the coated samples, deformation occurred in the form of brittle fracture, and the depth reached 15 µm due to crack propagation. It can be assumed that the high hardness values created by W_2C started after this depth and crack propagation stopped (Fig. 7).

On the other hand, the wear widths in the coated samples were at a minimum level compared to the uncoated samples. This shows that the abrasive ball could penetrate the coating superficially. However, as mentioned above, the capillary cracks formed under pressure on the hard layer progressed deep into the material under repeated load. This effect is negligible when the total coating thickness is taken into account. The regular wear forms on the uncoated samples suggest that the rolling sphere deformed the rail material in an abrasive form (Fig. 9.a and Fig. 9.b). The observed form is expected when the rail hardness (260 HV) is compared with the hardness of the abrasive ball (505 HV). The roughnesses formed on the wear profile line in Fig. 9.b can be expressed

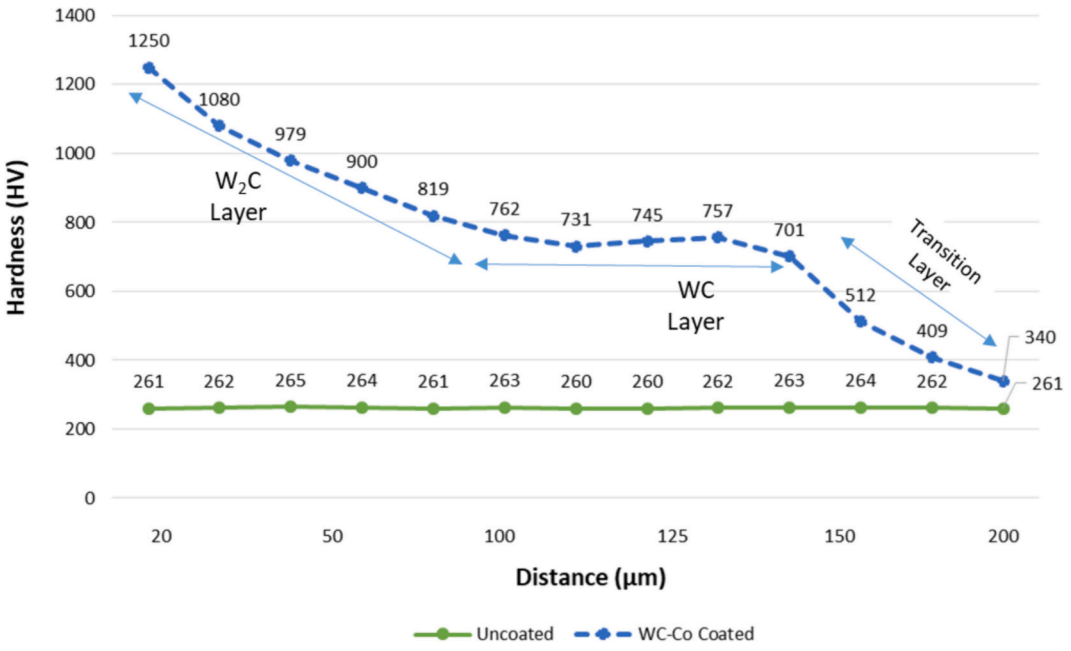

Fig. 7. Hardness graph of coated and uncoated rail steel samples.

as the points where the water film is interrupted under the effect of pressure (Semi-liquid friction state). According to Fig. 9.c and d, the wear mechanism formed in the coated samples can be defined as rapid fatigue wear. The cracks formed under repeated load progressed very quickly depending on the hardness. Although this situation seems like a catastrophic deformation, no problems occurred in terms of the reliability of the coating thanks to the crack propagation-stopping mechanisms in the lower layer.

The SEM images obtained for the analysis of wear mechanisms are given in Fig. 10. Fig. 10 shows the wear track widths of the coated and uncoated samples. The contact points between the abrasive ball and the rail material have decreased thanks to the tribofilm layer formed by the water. In the SEM image of the uncoated sample given in Fig. 10.a, it is seen that an aggressive abrasive wear mechanism has formed. In addition to the relative motion between the 100Cr6 ball and the rail steel, the stress acting on the rail steel creates the shear fracture (mode II) mechanism, which causes plastic deformation on the material's surface. The increase in stress due to the continuity of relative motion causes the atomic planes in the rail steel to shift and the interatomic bonds to break. This reduces the fracture toughness of the material, creating catastrophic wear deformations in the uncoated sample. While a regular friction track formation was observed in the centre of the deformation area, irregular formations were observed in the edge regions of the track. These irregular formations can be explained by the adhesive and ploughing effects created by the particles breaking away from the centre region. It can be claimed that more than one wear mechanism is effective due to excessive entropy in the dry friction environment. Still, the wear is predominantly abrasive due to the stable boundaries in the centre track. In Fig. 10.b, it is seen that a more superficial abrasive wear mechanism has formed compared to the dry environment (Fig. 10.a) due to the liquid film effect. In the images of WC-coated samples given in Figs. 10.c and 10.d, flaking mechanisms occur on the surface. Flaking wear is frequently observed in rail wheel systems due to fatigue [72,73]. The capillary cracks formed by the effect of tangential and radial forces on the rail surface widen due to repeated load and are effective in the formation of the flaking mechanism [1]. However, it is seen that the flaking formed in Fig. 10.c is more superficial compared to the flaking images in the literature. The increase in the hardness of the material by the WC coating reduces the elastic strain energy acting on the material and the formation of cracked surfaces. This ensures that the deformation level is superficial on WC-coated surfaces compared to uncoated surfaces. In addition, the metallurgical properties of the coating layer are also of great importance in terms of wear resistance. It is seen in the SEM images given in Fig. 4 that the void and crack defects formed in the coating obtained with the HVOF method are at a minimum level. The minimum discontinuities in the coating layer and the low W_2C brittle phase ratio (Fig. 6) increased the strength of the coating. Since the increase in hardness formed by the effect of WC coating makes plastic deformation difficult, flaking has decreased. This situation shows that the service life of WC-coated rails will increase. According to the image in Fig. 10.d, the flaking defect has increased in the WC-coated rail sample under pure water. Although the wear scar width has decreased due to the effect of the fluid, the flaking has become apparent due to the formation of a semi-liquid film layer. The excessive pressure formed at the points where the film layer was torn has caused the formation of welds, and therefore, the surface colour tone has darkened. Tangential forces acting on micron-sized weld points caused the weld to break and more flaking defects to occur. However, the fact that the wear scar width is small and the flaking occurs in a superficial form indicates that the film layer has a protective effect.

Fig. 11 shows the topography images obtained from the wearing surfaces. Topography images were considered to verify the results obtained from the friction coefficient, volume loss and SEM images. The Ra and Sa values in Fig. 11 are consistent with the other analysis parameters. The fact that Ra and Sa were obtained in numerically small values (< 0.4 µm) indicates that abrasive mechanism-based deformation has occurred between the abrasive ball and the rail material. In Fig. 11, red regions represent peak points, blue regions represent valley points, and yellow and green regions indicate minimum surface roughness. The morphology of Fig. 11.a shows that the rail steel is subjected to intense deformation under sliding friction. According to the SEM images, the red regions confirm the claimed adhesion and ploughing mechanisms. Again, the aggressive abrasion image determined by SEM images is noticeable in the midline of the figure. The morphology of the uncoated rail steel under pure water shows the existence of the abrasive wear mechanism in planar form (Fig. 11.b). Fig. 11.c shows that the rough surface form is formed due to dry wear conditions. According to the SEM images, the claimed flaking mechanisms are not clearly seen in the 3D topography images. However, the lack of red and blue tones shows that the WC coating increases the wear resistance and reduces material loss.

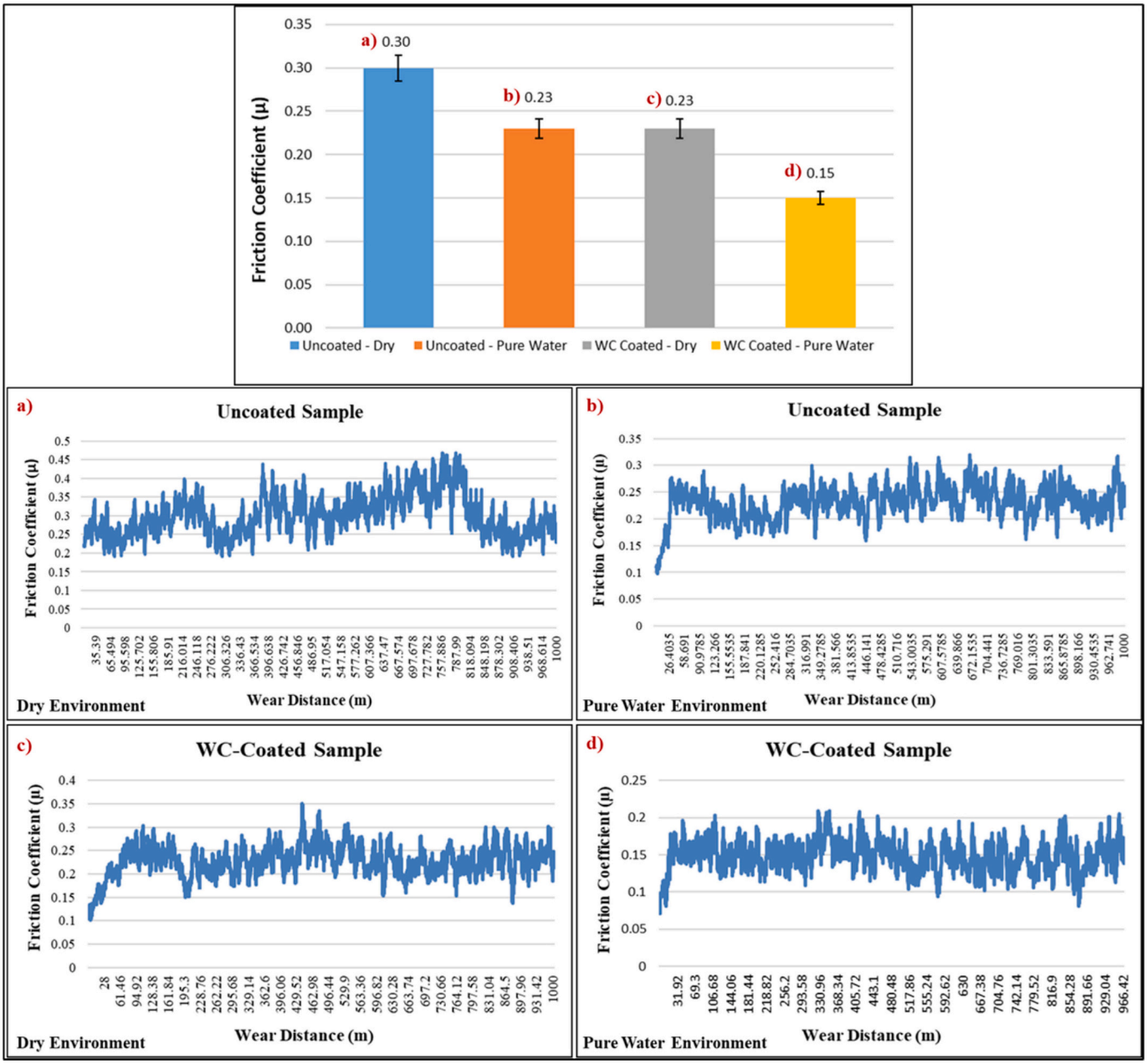

Fig. 8. Friction coefficient values under different test conditions.

In Fig. 11.d, it is seen that minimum deformation occurs on the surface of the WC-coated rail steel under pure water conditions. Thanks to the hardness of the coating and the liquid film layer, the surface appears planar with green and yellow tones. It can be claimed that the discontinuity of the liquid film layer causes the fluctuations on the surface. The high temperature and adhesion problems in the areas where the fluid film is torn have caused micron-level fluctuations on the surface.

Rails are exposed to massive loads due to operating conditions and operate in environments open to the atmosphere. Massive loads acting on rails create variable stresses in axial and radial directions (Fig. 12). While these stresses do not create aggressive deformations due to rolling friction in linear railway lines, they cause serious shear stresses and deformations, especially in curves and switch transitions. For this reason, it is noteworthy to provide protection with coating in sections where catastrophic wear defects occur.

With the average hardness values of 1200 HV obtained on the rails with WC coating, the coefficient of friction and mass loss values have decreased, and the surface morphology has improved. The results are to increase the service life of the rails. The value of 1200 HV is accepted as glassy hardness. In railways, it is desired that the rail and wheel hardnesses are close in order to minimise wheel wear. For this reason, applying WC coating to the entire rails is not meaningful in terms of technical and operating conditions. It has been determined that WC coating is an important solution in areas where catastrophic wear is seen. The fact that the coating thickness can be made at 150 μm is also valuable in terms of the long service life of the coating. The fact that the WC coating has a bcc structure in stoichiometric conditions has provided a high amount of diffusion to the rail steel in the pearlitic structure. Generally, the fact that hard coatings have a complex lattice structure (orthorhombic, tetragonal, rhombohedra) creates problems in terms of material compatibility, and there are problems in terms of application method and binding element reinforcement. In the WC coating process, only the Co element is used as a binder. The Co element is an important steel alloy element and ensures that the transition area between the

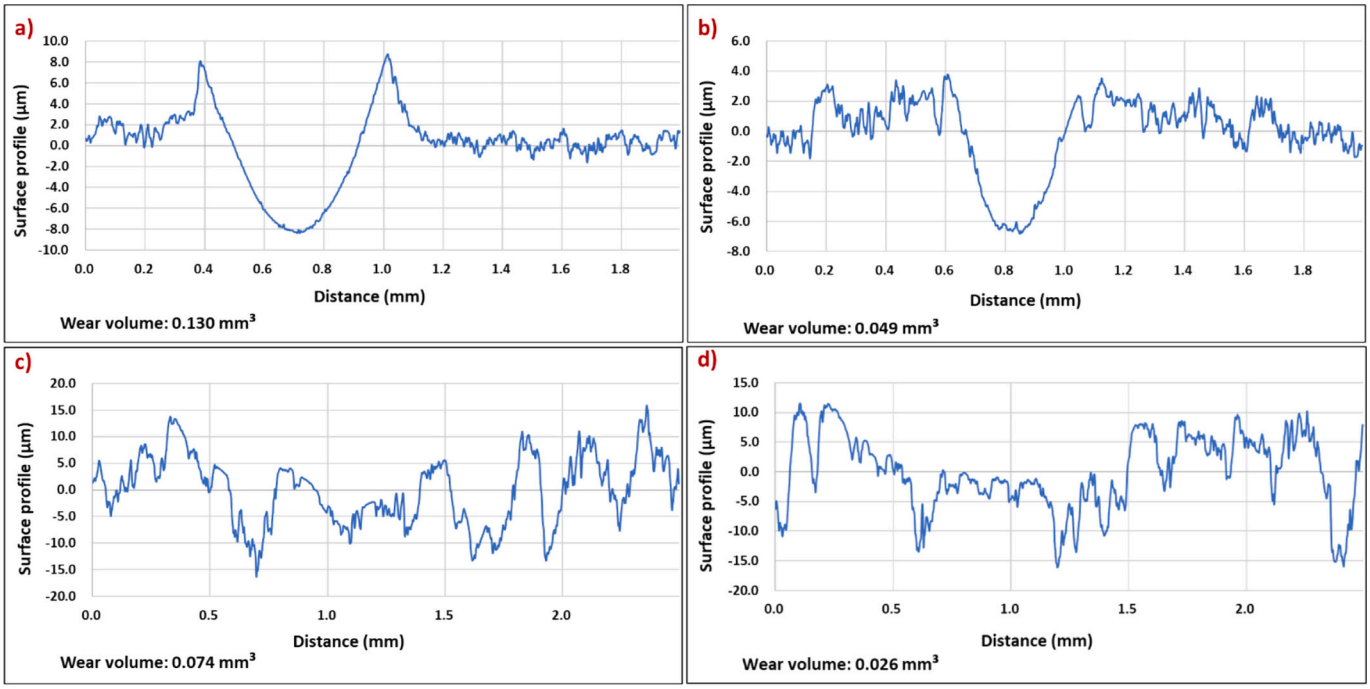

Fig. 9. 2D profilometer roughness values (a) uncoated sample in a dry environment (b) uncoated sample in the pure water environment (c) WC coated sample in a dry environment (d) WC coated sample in the pure water environment.

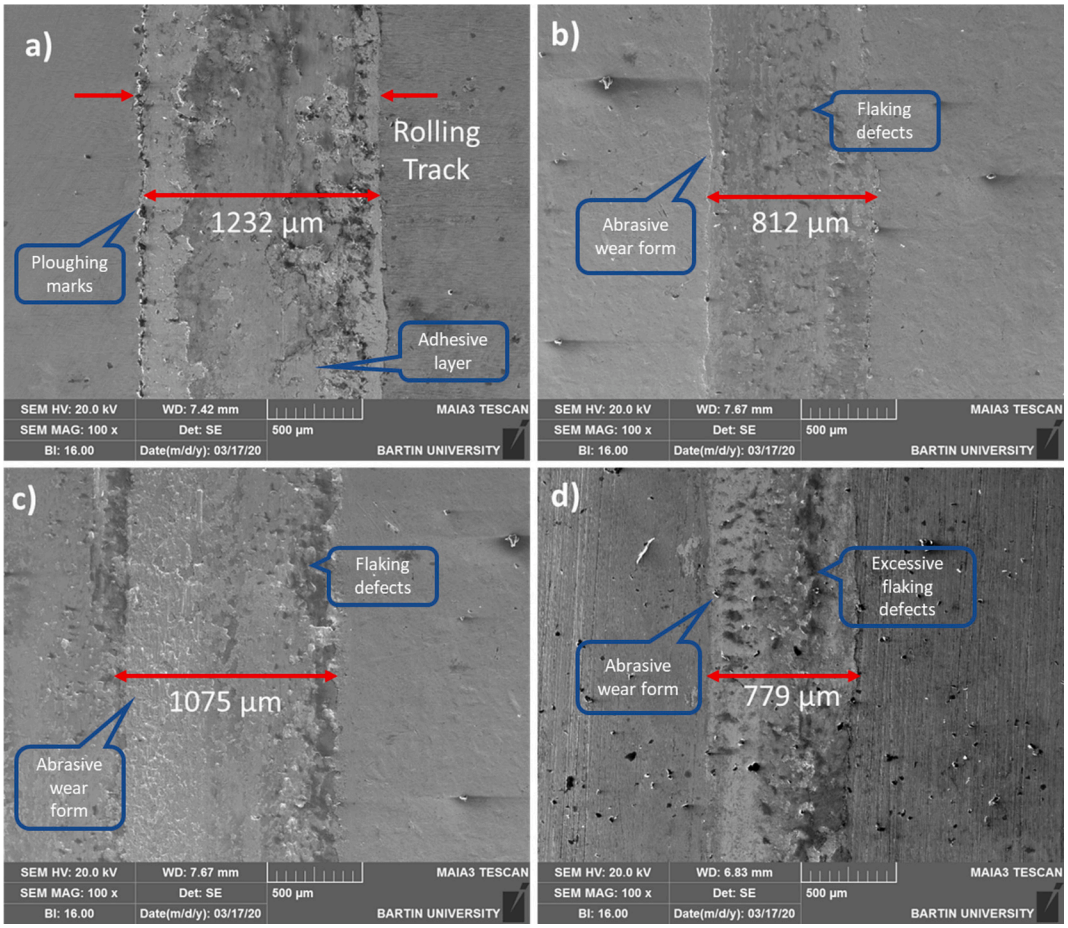

Fig. 10. SEM image of wear mechanisms (a) uncoated sample in a dry environment (b) uncoated sample in pure water environment (c) WC coated sample in a dry environment (d) WC coated sample in pure water environment.

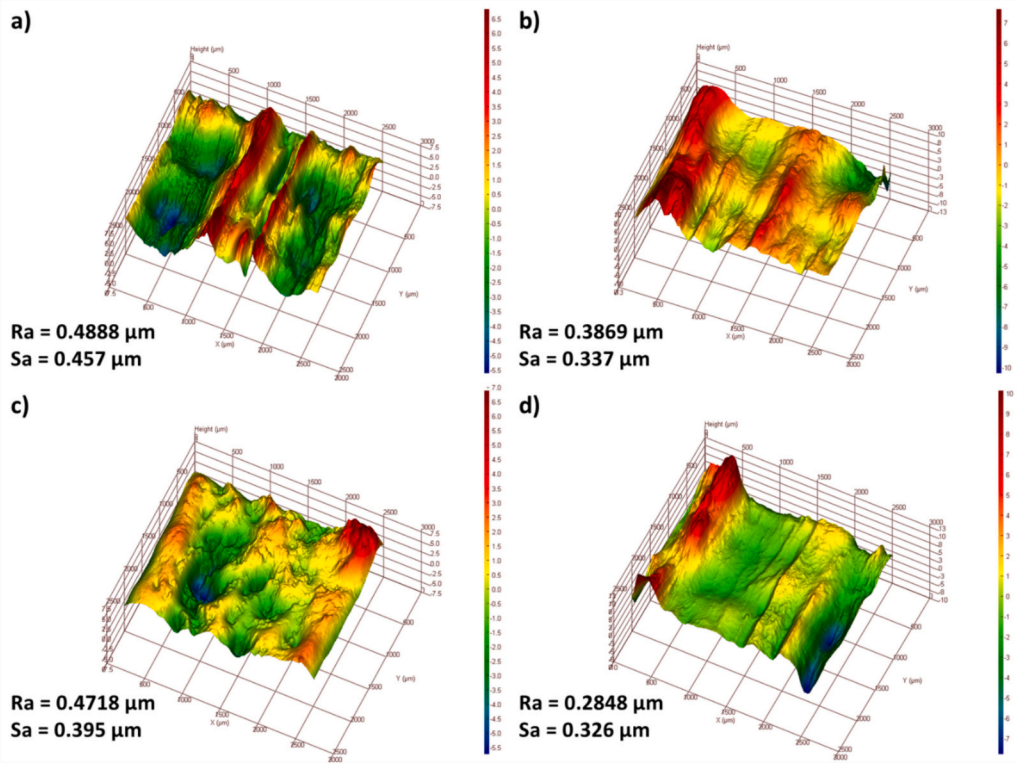

Fig. 11. 3D profilometer images (a) uncoated sample in a dry environment (b) uncoated sample in the pure water environment (c) WC coated sample in a dry environment (d) WC coated sample in the pure water environment.

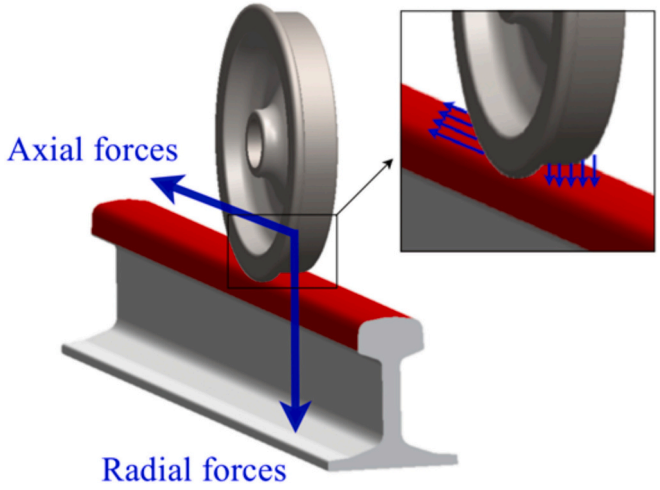

Fig. 12. Loads acting on railway steel during transportation.

coating and the rail steel is formed to prevent stress concentration.

The preference of the HVOF method in the coating process of rail steels has yielded significant results. It is important that the HVOF process is carried out at approximately 2500 K values and supersonic speeds in order to prevent WC particles from oxidising during transfer. The penetration of oxide particles into the rail is a risk factor in terms of crack formation and progression in rails exposed to repeated loads. Although WC is a chemically stable compound, there is a possibility that the Co element may bond with atmospheric gases. The results obtained from elemental analyses show that no problem occurs regarding oxide formation. After the coating layer is formed, the cooling rates of the material and the coating layer also affect the mechanical and metallurgical properties. It is thought that the coating layer is subjected to very rapid cooling at room temperature conditions starting from the outermost surface, while the rail material cools in a controlled manner depending on the coating layer. It can be claimed that the very hard W_2C layer is formed at this stage due to decarburisation. However, this layer is formed only on the outer surface and is a few microns thick, and then the WC layer is formed throughout the coating thickness. Under operating conditions, the extremely hard W_2C layer is expected to deform in a short time due to low toughness, but the WC layer is expected to protect the railhead for a long time.

3.3. Corrosion performance of the WC layer under dry and pure water conditions

In this study, the corrosion behaviour of uncoated and WC-coated railway steels was analysed through potentiodynamic polarisation tests. The corrosion resistance of both materials was evaluated and compared based on the Tafel polarisation curves (Fig. 13). Fig. 13 can be called a typical polarisation curve according to the literature [74]. The Tafel polarisation curves are represented by WC-coated rail steel in red and uncoated rail steel in black. With Tafel curves, important parameters like corrosion potential (Ecorr) and corrosion current density (Icorr), which are necessary to determine a material's corrosion resistance, are obtained. The corrosion current density (icorr), corrosion potential (Ecorr) and corrosion rate values obtained from the polarisation graphs are given in Table 3. Low icorr and corrosion rate and high Ecorr values indicate high corrosion resistance [75]. The WC-coated railway steel displayed a higher corrosion potential than the uncoated railway steel. This demonstrates that the WC coating increases railway steel's corrosion resistance and is more durable to corrosion wear. The corrosion current density is directly related to the corrosion rate. The WC-coated railway steel showed a lower Icorr value, representing a slower corrosion rate compared to the uncoated railway steel. This further confirms the improved corrosion resistance due to the WC coating. The Tafel polarisation curves demonstrate that the WC coating

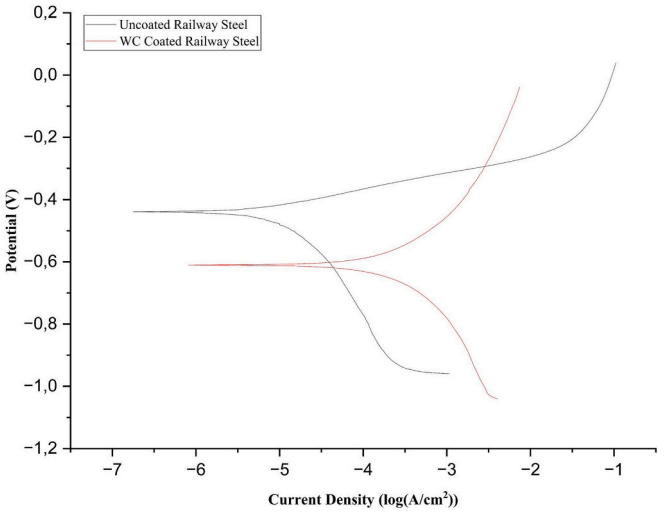

Fig. 13. Tafel polarisation curves.

significantly improves the corrosion resistance of rail steel. Uncoated railway steel has lower corrosion potential and higher corrosion current density and occurs in faster corrosion wear. In contrast, the WC coating enhances the corrosion potential and decreases the corrosion current density, thereby enhancing the railway steel's resistance to corrosion. The corrosion mechanism in WC-Co-coated samples occurs with the active electrochemical reaction at the cobalt matrix-carbide interface [76]. In the literature, it has been determined that the corrosion resistance increases in WC-12Co coating due to the homogeneous distribution of carbide particles [77]. In the current study, it can be claimed that the homogeneous distribution of carbide particles in the coating layer (Fig. 4) minimises the cobalt matrix-carbide interface and increases the corrosion resistance of the coating. These findings emphasise the impact of WC coatings in developing the corrosion properties of railway steels by protecting the coating/substrate interface [78]. While the high carbide content of rail steels increases corrosion resistance, the resistance ability is further increased with WC coating [79].

The SEM images obtained as a result of the potentiodynamic test for the analysis of deformations caused by corrosion are given in Fig. 14. It is seen that the area exposed to corrosion is wider in the uncoated sample compared to the WC coated sample. It is stated in the literature that rail steels with pearlitic structure have high corrosion resistance compared to rail steels with other microstructures [29]. In the current study, despite the high corrosion resistance of pearlitic rail steels, dense oxide layer formation is observed on the material surface under the effect of NaCl (Fig. 14.b). Although coating layers with low porosity are obtained on the surface of the WC-coated sample with the HVOF coating method, it is impossible to prevent porosity formation [48,53] completely. It is thought that corrosion mechanisms occur only in porosity areas due to the discontinuity of the coating layer (Fig. 14.d). The fact that the corrosive effect does not occur in areas other than the porosity areas or that it occurs superficially can be explained by the corrosion resistance of the WC coating. Thanks to the coating, the purity of the material surface is reduced and this increases the corrosion resistance. It has been stated in the literature that in low-purity materials, continuity cannot be achieved as a result of the oxide layer encountering secondary phases [60]. Due to discontinuity, the surface area exposed to corrosive effects decreases. The oxygen amounts in the EDX images of coated and uncoated samples also prove the claim that WC coating reduces oxide layer formation by increasing corrosion resistance (Fig. 15). Additionally, it can be claimed that crack formation and propagation mechanisms in the base material can be minimised with the coating layer [80–82]. It can be claimed that WC coating is as effective in corrosion resistance as multi-principle element alloys

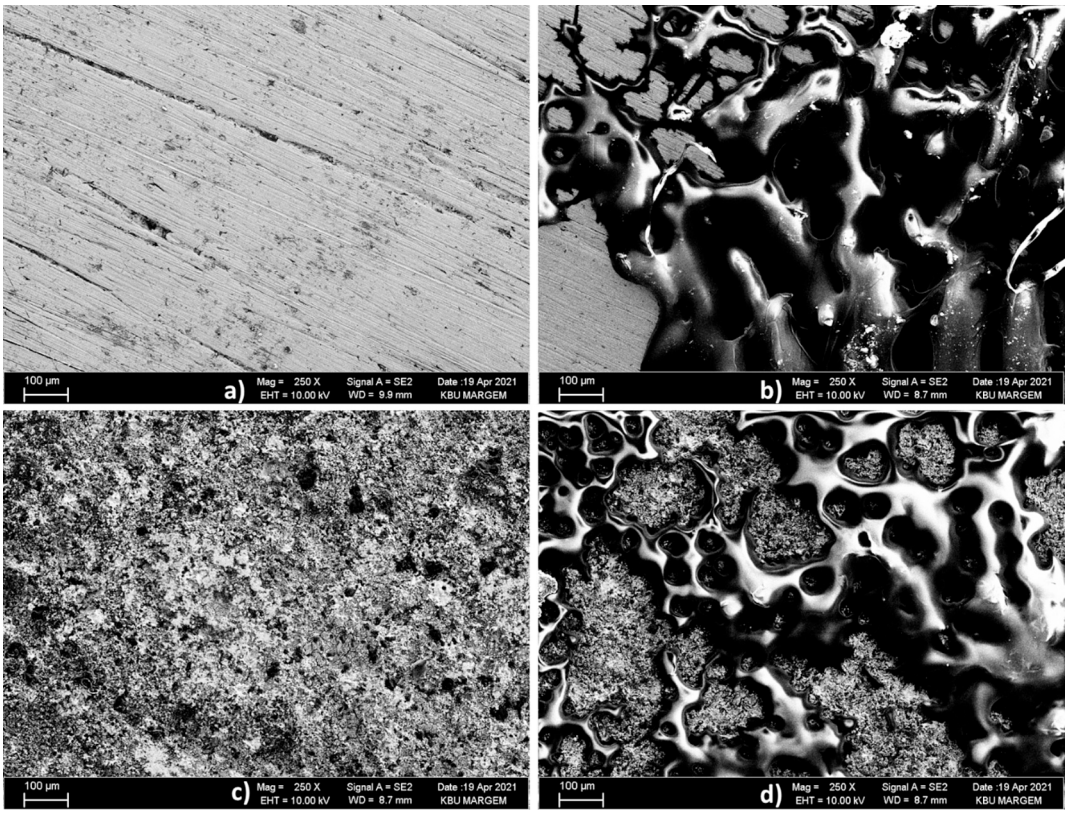

Fig. 14. Corrosion test SEM images (a) uncoated sample in a dry environment (b) uncoated sample in the pure water environment (c) WC coated sample in a dry environment (d) WC coated sample in the pure water environment.

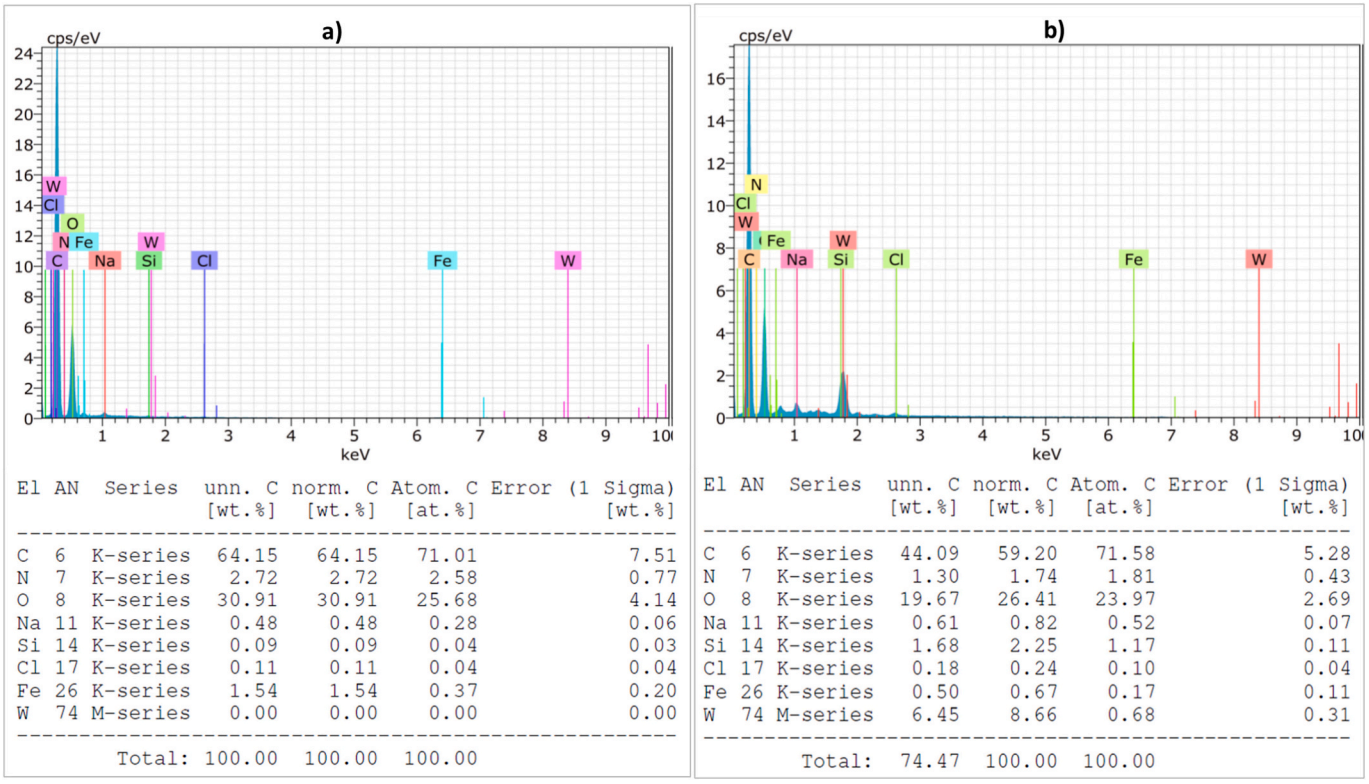

El	AN	Series	unn. C [wt.%]	norm. C [wt.%]	Atom. C [at.%]	Error (1 Sigma) [wt.%]
C	6	K-series	64.15	64.15	71.01	7.51
N	7	K-series	2.72	2.72	2.58	0.77
O	8	K-series	30.91	30.91	25.68	4.14
Na	11	K-series	0.48	0.48	0.28	0.06
Si	14	K-series	0.09	0.09	0.04	0.03
Cl	17	K-series	0.11	0.11	0.04	0.04
Fe	26	K-series	1.54	1.54	0.37	0.20
W	74	M-series	0.00	0.00	0.00	0.00
		Total:	100.00	100.00	100.00	

El	AN	Series	unn. C [wt.%]	norm. C [wt.%]	Atom. C [at.%]	Error (1 Sigma) [wt.%]
C	6	K-series	44.09	59.20	71.58	5.28
N	7	K-series	1.30	1.74	1.81	0.43
O	8	K-series	19.67	26.41	23.97	2.69
Na	11	K-series	0.61	0.82	0.52	0.07
Si	14	K-series	1.68	2.25	1.17	0.11
Cl	17	K-series	0.18	0.24	0.10	0.04
Fe	26	K-series	0.50	0.67	0.17	0.11
W	74	M-series	6.45	8.66	0.68	0.31
		Total:	74.47	100.00	100.00	

Fig. 15. Corrosion test EDX results.

(TiZrHfNb) [83]. Increasing corrosion resistance is important for the conservation of materials and energy in the national economy [84].

4. Conclusions

In this study, the effect of WC-Co coating on the wear and corrosion resistance of rail steels was investigated. The results obtained are given below.

- When the SEM images of the coated surfaces were examined, it was found that the coating thickness was ~165 μm, and according to the microhardness measurement results, the hardness values in the regions where WC and W_2C phases were formed were ~ 750 HV and ~ 1250 HV, respectively.
- Thanks to the coating process, the friction coefficient has decreased by an average of 30 % in both wet and dry conditions. The obtained value is important in terms of the applicability of WC coating on rails exposed to wear.
- After the WC coating process, the wear volume value decreased by 46.94 % in the wet environment and by 43.07 % in the dry environment.
- According to the Ecorr, icorr and corrosion rate values obtained from the polarisation graphs, it was determined that the corrosion potential of uncoated samples was lower, and the corrosion rate was higher compared to the coated samples.

Author contribution

All authors contributed to this study. [Orak, A., Korkmaz, S. And Cetin, M. H.] developed the research idea and designed the study. [Orak, A.] managed the data collection process and performed the analyses. All authors interpreted the data and carried out the writing process of the article. All authors reviewed and approved the study for approval of the final version.

Ethics approval and permissions

This study does not require ethics committee approval.

Data access and sharing

The data used in this study are available upon request to ensure verification of the research results.

Declaration of generative AI and AI-assisted technologies in the writing process

In the preparation of this work, A.O. utilized GPT-3.5 by OpenAI to enhance language and readability, applying it with caution. Following the use of this tool, the author carefully reviewed and edited the content, taking full responsibility for the final version of the publication.

Funding statement

This research was not supported by any institution. The findings and conclusions obtained in the study represent the views of the authors only.

Declaration of competing interest

The authors declare that there is no financial or personal conflict of interest that could affect the outcome of the study.

Data availability

The data that has been used is confidential.

References

[1] J. Pan, L. Chen, C. Liu, et al., Relationship between the microstructural evolution and wear behavior of U71Mn rail steel, J. Mater. Eng. Perform. [Internet] 30 (2021) 1090–1098. Available from: https://doi.org/10.1007/s11665-021-05452-6.

[2] R. Lewis, P. Christoforou, W.J. Wang, et al., Investigation of the influence of rail hardness on the wear of rail and wheel materials under dry conditions (ICRI wear mapping project), Wear [Internet] 430–431 (2019) 383–392. Available from: https://doi.org/10.1016/j.wear.2019.05.030.

[3] O. Yazici, S. Yilmaz, Investigation of effect of various processing temperatures on abrasive Wear behaviour of high power diode laser treated R260 grade rail steels, Tribol. Int. [Internet] 119 (2018) 222–229. Available from: https://doi.org/10.1016/j.triboint.2017.11.006.

[4] L. Deters, M. Proksch, Friction and wear testing of rail and wheel material, Wear 258 (2005) 981–991.

[5] S.M. Hasan, D. Chakrabarti, S.B. Singh, Dry rolling/sliding wear behaviour of pearlitic rail and newly developed carbide-free bainitic rail steels, Wear [Internet] 408–409 (2018) 151–159. Available from: https://doi.org/10.1016/j.wear.2018.05.006.

[6] B. Panda, R. Balasubramaniam, A. Moon, Microstructure and mechanical properties of novel rail steels, Mater. Sci. Technol. 25 (2009) 1375–1382.

[7] R. Stock, R. Pippan, RCF and Wear in theory and practice-the influence of rail grade on wear and RCF, Wear [Internet] 271 (2011) 125–133. Available from: https://doi.org/10.1016/j.wear.2010.10.015.

[8] S. Samal, A. Bhattaacharyya, S.K. Mitra, Study on corrosion behavior of Pearlitic rail steel, J. Miner. Mater. Charact. Eng. 10 (2011) 573–581.

[9] J.W. Seo, H.K. Jun, S.J. Kwon, et al., Rolling contact fatigue and wear of two different rail steels under rolling-sliding contact, Int. J. Fatigue [Internet] 83 (2016) 184–194. Available from: https://doi.org/10.1016/j.ijfatigue.2015.10.012.

[10] B. Panda, R. Balasubramaniam, G. Dwivedi, et al., Corrosion of novel rail steels in 3.5% NaCl solution, Trans. Indian Inst. Metals 61 (2008) 177–181.

[11] A. Mazzù, L. Solazzi, M. Lancini, et al., An experimental procedure for surface damage assessment in railway wheel and rail steels, Wear [Internet] 342–343 (2015) 22–32. Available from: https://doi.org/10.1016/j.wear.2015.08.006.

[12] G. Donzella, M. Faccoli, A. Ghidini, et al., The competitive role of wear and RCF in a rail steel, Eng. Fract. Mech. 72 (2005) 287–308.

[13] S.S. Sahay, G. Mohapatra, G.E. Totten, Overview of pearlitic rail steel: accelerated cooling, quenching, microstructure and mechanical properties, J. ASTM Int. (2009) 6.

[14] S.M. Shariff, T.K. Pal, G. Padmanabham, et al., Sliding wear behaviour of laser surface modified Pearlitic rail steel, Surf. Eng. 26 (2010) 199–208.

[15] S. Maya-Johnson, J. Felipe Santa, A. Toro, Dry and lubricated Wear of rail steel under rolling contact fatigue - Wear mechanisms and crack growth, Wear [Internet] 380–381 (2017) 240–250. Available from: https://doi.org/10.1016/j.wear.2017.03.025.

[16] Y. Lyu, Y. Zhu, U. Olofsson, Wear between wheel and rail: a pin-on-disc study of environmental conditions and iron oxides, Wear [Internet] 328–329 (2015) 277–285. Available from: https://doi.org/10.1016/j.wear.2015.02.057.

[17] D. Nikas, K.A. Meyer, J. Ahlström, Characterization of deformed pearlitic rail steel, IOP Conf. Ser. Mater. Sci. Eng. 219 (2017).

[18] A.R. Khan, Y. Shengfu, H. Wang, Influence of heat input and preheating on microstructure and mechanical properties of coarse grain heat-affected zone of metal arc gas-welded Pearlitic rail steel, J. Mater. Eng. Perform. [Internet] 28 (2019) 7676–7686. Available from: https://doi.org/10.1007/s11665-019-04486-1.

[19] R. Stock, R. Pippan, Rail grade dependent damage behaviour - characteristics and damage formation hypothesis, Wear [Internet] 314 (2014) 44–50. Available from: https://doi.org/10.1016/j.wear.2013.11.029.

[20] F.A.M. Alwahdi, A. Kapoor, F.J. Franklin, Subsurface microstructural analysis and mechanical properties of pearlitic rail steels in service, Wear [Internet] 302 (2013) 1453–1460. Available from: https://doi.org/10.1016/j.wear.2012.12.058.

[21] D. Nikas, J. Ahlström, A. Malakizadi, Mechanical properties and fatigue behaviour of railway wheel steels as influenced by mechanical and thermal loadings, Wear [Internet] 366–367 (2016) 407–415. Available from: https://doi.org/10.1016/j.wear.2016.04.009.

[22] A. Çelik, Demiryolu Ray ve Kusurlarını Tespit Etmek İçin Geliştirilen İki Yeni Yöntem, Demiryolu Mühendisliği (2020) 52–63.

[23] M.A. Sevim, A.C. Çelt, S. Kabar, et al., Demiryollarında Raylara Uygulanan Tahribatsız Muayene Yöntemleri, Demiryolu Mühendisliği (2020) 60–74.

[24] B. Kalyoncuoğlu, Mantarı Sertleştirilmiş Rayların Kırılma Mekaniği Özelliklerinin İncelenmesi, Karabük Üniversitesi, 2016.

[25] S. Altun, Isıl İşlem Görmüş Ray çeliğinin Aşınma Davranışlarının İncelenmesi, Mersin Üniversitesi, 2019.

[26] G. Donzella, A. Mazzù, C. Petrogalli, Competition between Wear and rolling contact fatigue at the wheel-rail Interface: some experimental evidence on rail steel, Proc. Inst. Mech. Eng. Part F J. Rail Rapid Transit. 223 (2009) 31–44.

[27] J. Herian, K. Aniolek, Abrasive Wear of railway sections of steel with a different pearlite morphology in railroad switches, J. Achiev. Mater. Manuf. Eng. 43 (2010) 236–243.

[28] C. Dayot, A. Saulot, C. Godeau, et al., Tribological behaviour of Pearlitic and Bainitic steel grades under various sliding conditions, Tribol. Int. [Internet] 46 (2012) 128–136. Available from: https://doi.org/10.1016/j.triboint.2011.05.016.

[29] P.K. Katiyar, S. Misra, K. Mondal, Comparative corrosion behavior of five microstructures (pearlite, Bainite, Spheroidized, Martensite, and tempered Martensite) made from a high carbon steel, Metall. Mater. Trans. A Phys. Metall Mater. Sci. [Internet] 50 (2019) 1489–1501. Available from: https://doi.org/10.1007/s11661-018-5086-1.

[30] M.A. Gómez-Guarneros, J.G. Godínez-Salcedo, E.A. Gallardo-Hernández, et al., Corrosion rate and mechanisms of a rail head surface under artificial rainwater conditions, Mater. Lett. 287 (2021) 1–6.

[31] C.C. Viáfara, M.I. Castro, J.M. Vélez, et al., Unlubricated sliding Wear of Pearlitic and Bainitic steels, Wear 259 (2005) 405–411.

[32] S. Sharma, S. Sangal, K. Mondal, Wear behaviour of bainitic rail and wheel steels, Mater. Sci. Technol. 32 (2016) 266–274.

[33] P.K. Katiyar, S. Misra, K. Mondal, Comparative corrosion behavior of five microstructures (pearlite, Bainite, Spheroidized, Martensite, and tempered Martensite) made from a high carbon steel, Metall. Mater. Trans. A Phys. Metall. Mater. Sci. 50 (2019) 1489–1501.

[34] J.W. Seo, J.C. Kim, S.J. Kwon, et al., Effects of laser cladding for repairing and improving wear of rails, Int. J. Precis Eng. Manuf. [Internet] 20 (2019) 1207–1217. Available from: https://doi.org/10.1007/s12541-019-00115-y.

[35] A. Saulot, S. Descartes, D. Desmyter, et al., A tribological characterization of the “damage mechanism” of low rail corrugation on sharp curved track, Wear 260 (2006) 984–995.

[36] J.W. Seo, J.C. Kim, S.J. Kwon, et al., Effects of laser cladding for repairing and improving wear of rails, Int. J. Precis. Eng. Manuf. 20 (2019) 1207–1217.

[37] S.R. Lewis, S. Fretwell-Smith, P.S. Goodwin, et al., Improving rail wear and RCF performance using laser cladding, Wear [Internet] 366–367 (2016) 268–278. Available from: https://doi.org/10.1016/j.wear.2016.05.011.

[38] Guo H. Ming, Q. Wang, Wang W. Jian, et al., Investigation on wear and damage performance of laser cladding co-based alloy on single wheel or rail material, Wear [Internet] 328–329 (2015) 329–337. Available from: https://doi.org/10.1016/j.wear.2015.03.002.

[39] W.J. Wang, Z.K. Fu, J. Guo, et al., Investigation on Wear resistance and fatigue damage of laser cladding coating on wheel and rail materials under the oil lubrication condition, Tribol. Trans. 59 (2016) 810–817.

[40] Guo H. Ming, Q. Wang, Wang W. Jian, et al., Investigation on Wear and damage performance of laser cladding co-based alloy on single wheel or rail material, Wear (2015) 328–329, 329–337.

[41] Z.K. Fu, H.H. Ding, W.J. Wang, et al., Investigation on microstructure and Wear characteristic of laser cladding Fe-based alloy on wheel/rail materials, Wear 330–331 (2015) 592–599.

[42] W.J. Wang, J. Hu, J. Guo, et al., Effect of laser cladding on wear and damage behaviors of heavy-haul wheel/rail materials, Wear 311 (2014) 130–136.

[43] A.T. Clare, O. Oyelola, T.E. Abioye, et al., Laser cladding of rail steel with Co-Cr, Surf. Eng. 29 (2013) 731–736.

[44] S.R. Lewis, S. Fretwell-Smith, P.S. Goodwin, et al., Improving rail Wear and RCF performance using laser cladding, Wear 366–367 (2016) 268–278.

[45] M. Federici, C. Menapace, A. Moscatelli, et al., Effect of roughness on the Wear behavior of HVOF coatings dry sliding against a friction material, Wear [Internet] 368–369 (2016) 326–334. Available from: https://doi.org/10.1016/j.wear.2016.10.013.

[46] L. Qiao, Y. Wu, S. Hong, et al., Wet abrasive Wear behavior of WC-based cermet coatings prepared by HVOF spraying, Ceram Int. [Internet] 47 (2021) 1829–1836. Available from: https://doi.org/10.1016/j.ceramint.2020.09.009.

[47] T.K. Mishra, A. Kumar, S.K. Sinha, Experimental investigation and study of HVOF sprayed WC-12Co, WC-10Co-4Cr and Cr3C2-25NiCr coating on its sliding Wear behaviour, Int. J. Refract. Met. Hard Mater. [Internet] 94 (2021) 1–15. Available from: https://doi.org/10.1016/j.ijrmhm.2020.105404.

[48] J. Schubert, Š. Houdková, M. Kašparová, et al., Effect of Co content on the properties of HVOF sprayed coatings based on tungsten carbide, in: Met 2013 - 22nd Int Conf Metall Mater Conf Proc, 2013, pp. 1100–1105.

[49] A.K. Basak, J.P. Celis, M. Vardavoulias, et al., Effect of Nanostructuring and Al alloying on friction and Wear behaviour of thermal sprayed WC-co coatings, Surf. Coat. Technol. [Internet] 206 (2012) 3508–3516. Available from: https://doi.org/10.1016/j.surfcoat.2012.02.030.

[50] V. Rajinikanth, K. Venkateswarlu, An investigation of sliding wear behaviour of WC-co coating, Tribol. Int. [Internet] 44 (2011) 1711–1719. Available from: https://doi.org/10.1016/j.triboint.2011.06.021.

[51] Q. Yang, T. Senda, A. Hirose, Sliding wear wehavior of WC-12% co coatings at elevated temperatures, Surf. Coat. Technol. 200 (2006) 4208–4212.

[52] B. Somasundaram, B.C. Navinesh, Jegadeeswaran, et al., Wear behavior of HVOF sprayed WC-Co/NiCrAlYSi (35–65%) and WC-Co/NiCrAlYSi (80–20%) coatings on turbine SS316 steel, Mater. Today Proc. [Internet] 20 (2020) 103–107. Available from: https://doi.org/10.1016/j.matpr.2019.10.048.

[53] M. Xie, S. Zhang, M. Li, Comparative investigation on HVOF sprayed carbide-based coatings, Appl. Surf. Sci. [Internet] 273 (2013) 799–805. Available from: https://doi.org/10.1016/j.apsusc.2013.03.010.

[54] T. Sahraoui, S. Guessasma, M. Ali Jeridane, et al., HVOF sprayed WC-Co coatings: microstructure, mechanical properties and friction moment prediction, Mater. Des. [Internet] 31 (2010) 1431–1437. Available from: https://doi.org/10.1016/j.matdes.2009.08.037.

[55] P. Chivavibul, M. Watanabe, S. Kuroda, et al., Effects of carbide size and Co content on the microstructure and mechanical properties of HVOF-sprayed WC-Co coatings, Surf. Coat. Technol. 202 (2007) 509–521.

[56] Q. Wang, Z.H. Chen, Z.X. Ding, Performance of abrasive wear of WC-12Co coatings sprayed by HVOF, Tribol. Int. 42 (2009) 1046–1051.

[57] M. Xie, S. Zhang, M. Li, Comparative investigation on HVOF sprayed carbide-based coatings, Appl. Surf. Sci. 273 (2013) 799–805.

[58] N. Vashishtha, R.K. Khatirkar, S.G. Sapate, Tribological behaviour of HVOF sprayed WC-12Co, WC-10Co-4Cr and Cr3C2−25NiCr coatings, Tribol. Int.

[Internet] 105 (2017) 55–68. Available from: https://doi.org/10.1016/j.triboint.2016.09.025.
[59] A. Mateen, G.C. Saha, T.I. Khan, et al., Tribological behaviour of HVOF sprayed near-nanostructured and microstructured WC-17wt.%Co coatings, Surf. Coat. Technol. [Internet] 206 (2011) 1077–1084. Available from: https://doi.org/10.1016/j.surfcoat.2011.07.075.
[60] M. Jalali Azizpour, M. Tolouei-Rad, The effect of spraying temperature on the corrosion and Wear behavior of HVOF thermal sprayed WC-Co coatings, Ceram Int. [Internet] 45 (2019) 13934–13941. Available from: https://doi.org/10.1016/j.ceramint.2019.04.091.
[61] J.L. Viesca, S. González-Cachón, A. García, et al., Tribological behaviour of microalloyed and conventional C–Mn rail steels in a pure sliding condition, Proc. Inst. Mech. Eng. Part F J. Rail Rapid Transit. 232 (2018) 2201–2214.
[62] U. Ozsarac, S. Aslanlar, Wear behaviour investigation of wheel/rail interface in water lubrication and dry friction, Ind. Lubr. Tribol. 60 (2008) 101–107.
[63] M. Faccoli, C. Petrogalli, A. Ghidini, A pin-on-disc study on the wear behaviour of two high-performance railway wheel steels, Tribol. Lett. 65 (2017) 1–7.
[64] B.N. Popov, Corrosion engineering: principles and solved problems, in: Corros. Eng. Princ. Solved Probl. South Carolina, Elsevier, 2015.
[65] W.D. Callister, D.G. Rethwisch, Materials Science and Engineering: An Introduction, Wiley, 2018.
[66] S. Korkmaz, M. Pehlivanoglu, A. Orak, et al., Investigation of wear behavior of carbide based coated rolling roll materials under dry and lubricated conditions, Surf. Topogr. Metrol. Prop. 9 (2021) 12–14.
[67] W.J. Wang, P. Shen, J.H. Song, et al., Experimental study on adhesion behavior of wheel/rail under dry and water conditions, Wear [Internet] 271 (2011) 2699–2705. Available from: https://doi.org/10.1016/j.wear.2011.01.070.
[68] F.J. Franklin, G.J. Weeda, A. Kapoor, et al., Rolling contact fatigue and wear behaviour of the Infrastar two-material rail, Wear 258 (2005) 1048–1054.
[69] J.P. Liu, Q.Y. Zhou, Y.H. Zhang, et al., The formation of Martensite during the propagation of fatigue cracks in Pearlitic rail steel, Mater. Sci. Eng. A 747 (2019) 199–205.
[70] R. He, J. Wang, M. He, et al., Synthesis of WC composite powder with Nano-cobalt coatings and its application in WC-4Co cemented carbide, Ceram. Int. 44 (2018) 10961–10967.
[71] E. Celik, O. Culha, B. Uyulgan, et al., Assessment of microstructural and mechanical properties of HVOF sprayed WC-based cermet coatings for a roller cylinder, Surf. Coat. Technol. 200 (2006) 4320–4328.
[72] H.C. Eden, J.E. Garnham, C.L. Davis, Influential microstructural changes on rolling contact fatigue crack initiation in Pearlitic rail steels, Mater. Sci. Technol. 21 (2005) 623–629.
[73] S. Maya-Johnson, J. Felipe Santa, A. Toro, Dry and lubricated Wear of rail steel under rolling contact fatigue - Wear mechanisms and crack growth, Wear [Internet] 380–381 (2017) 240–250. Available from: https://doi.org/10.1016/j.wear.2017.03.025.
[74] X. Meng, B. Zhang, F. Cao, Y. Liao, Effectiveness of measures on natural gas pipelines for mitigating the influence of DC ground current, IEEE Transactions on Power Delivery 39 (4) (2024 Aug) 2414–2423, https://doi.org/10.1109/TPWRD.2024.3406826.
[75] X. He, R.G. Song, D.J. Kong, Microstructure and corrosion behaviour of laser-cladding Al-Ni-TiC-CeO2 composite coatings on S355 offshore steel, J. Alloys Compd. 770 (2019) 771–783.
[76] J.M. Guilemany, J. Nin, C. Lorenzana, et al., Tribology of cermet/NiCrBSi coatings sprayed by HVOF, Boletín la Soc. Española Cerámica y Vidr. 43 (2004) 483–487.
[77] Miguel Ángel Reyes-Mojena, Roberto Carvajal Sagaro-Zamora, Hipólito Domingo Fals, V.A. Ferraresi, C.R.C. Lima, Tribocorrosion behaviour of cemented carbide coatings obtained by high velocity oxygen fuel spraying, Int. J. Surf. Sci. Eng. 9 (2015) 561–573.
[78] M. Bai, T. Liu, B. Liu, Y. Li, H. Yu, Y. Zhao, W. Liu, Preparation and properties of polyurethane cold galvanizing coatings with phosphoric acid modified zinc powder, Surf. Coat. Technol. 489 (2024) 131128.
[79] H. Wang, D. Qian, F. Wang, Z. Dong, J. Chen, Predictive mechanical property and fracture behavior in high-carbon steel containing high-density carbides via artificial RVE modeling, Mater. Des. 247 (2024) 113383.
[80] M. Huang, L. Wang, C. Wang, Y. Li, J. Wang, J. Yuan, W. Xu, Optimizing crack initiation energy in austenitic steel via controlled martensitic transformation, J. Mater. Sci. Technol. 198 (2024) 231–242.
[81] Z. Geng, C. Chen, M. Song, J. Luo, J. Chen, R. Li, K. Zhou, High strength Al0.7CoCrFeNi2. 4 hypereutectic high entropy alloy fabricated by laser powder bed fusion via triple-nanoprecipitation, J. Mater. Sci. Technol. 187 (2024) 141–155.
[82] X. Long, Y. Guo, Y. Su, K.S. Siow, C. Chen, Unveiling the damage evolution of SAC305 during fatigue by entropy generation, Int. J. Mech. Sci. 244 (2023) 108087.
[83] Y. Zhang, Z. Wang, S. Huang, H. Liu, Y. Yan, Electrochemical behavior and passivation film characterization of TiZrHfNb multi-principal element alloys in NaCl-containing solution, Corros. Sci. 235 (2024) 112185.
[84] R. Ji, Q. Zhao, L. Zhao, Y. Liu, H. Jin, L. Wang, Z. Xu, Study on high wear resistance surface texture of electrical discharge machining based on a new water-in-oil working fluid, Tribol. Int. 180 (2023) 108218.